Photoluminescent Green Carbon Nanodots from Food-Waste-Derived Sources: Large-Scale Synthesis, Properties, and Biomedical Applications

So Young Park,[†,‡] Hyun Uk Lee,*[†,‡] Eun Sik Park,[†,§] Soon Chang Lee,[⊥] Jae-Won Lee,[#] Soon Woo Jeong,[∥] Chi Hyun Kim,[∥] Young-Chul Lee,[Δ] Yun Suk Huh,[Δ] and Jouhahn Lee*[‡]

[‡]Division of Materials Science, Korea Basic Science Institute, Daejeon 305-333, Republic of Korea

[§]Korea Standards Research Institute of Food and Drug, Busan 607-120, Republic of Korea

[⊥]Department of Fine Chemical Engineering and Applied Chemistry, Chungnam National University, Daejeon 305-764, Republic of Korea

[#]Department of Energy Engineering, Dankook University, Cheonan 330-714, Republic of Korea

[∥]Bio & New Materials Business Team, National Nanofab Center, Daejeon 305-701, Republic of Korea

[Δ]Department of Biological Engineering, College of Engineering, Inha University, Incheon 402-751, Republic of Korea

S *Supporting Information*

ABSTRACT: We have developed a simple approach for the large-scale synthesis of water-soluble green carbon nanodots (G-dots) from many kinds of large food waste-derived sources. About 120 g of G-dots per 100 kg of food waste can be synthesized using our simple and environmentally friendly synthesis approach. The G-dots exhibit a high degree of solubility in water because of the abundant oxygen-containing functional groups around their surface. The narrow band of photoluminescence emission (400−470 nm) confirms that the size of the G-dots (∼4 nm) is small because of a similar quantum

effects and emission traps on the surfaces. The G-dots have excellent photostability; their photoluminescence intensity decreases slowly (∼8%) under continuous excitation with a Xe lamp for 10 days. We carried out cell viability assay to assess the effect of cytotoxicity by introducing G-dots in cells such as Chinese hamster ovary cells (CHO-K1), mouse muscle cells (C2C12), and African green monkey kidney cells (COS-7), up to a concentration of 2 mg mL^{-1} for 24 h. Due to their high photostability and low cytotoxicity, these G-dots are excellent probes for in vitro bioimaging. Moreover, the byproducts (not including G-dots) of G-dot synthesis from large food-waste derived sources promoted the growth and development of seedlings germinated on 3DW-supplemented gauze. Because of the combined advantages of green synthesis, high aqueous stability, high photostability, and low cytotoxicity, the G-dots show considerable promise in various areas, including biomedical imaging, solution state optoelectronics, and plant seed germination and/or growth.

KEYWORDS: *carbon nanodot, food waste, cytotoxicity, bioimaging, seed germination*

INTRODUCTION

Carbon-based nanomaterials have recently emerged as the most attractive candidates to produce alternative photoluminescent materials that do not contain toxic components such as heavy metals or semiconducting quantum dots.[1−3] These carbon-based nanomaterials such as fullerenes,[3] graphene oxide,[4] carbon nanotubes,[5] and carbon nanodots[6,7] are widely used in biomedical devices, such as optical sensor, medical diagnosis, and bioimaging probes enabled to offer size-dependent photoluminescence and chemical stability. However, the major concerns for these carbon-based nanomaterials are the limited water solubility, rapid photobleaching, and low photoluminescence efficiencies for biological applications.[1,6] Additionally, their potential adverse effects are unknown.[3,6]

Among the carbon-based materials, carbon nanodots have drawn the most extensive attention, because of their size-dependent photoluminescence emission, strong luminescence, and resistance to photobleaching.[1,3,6] The carbon nanodots have advantages over semiconductor quantum dots, such as low cost, high chemical- and photostability, and biocompatibility.[6−13] However, the traditional methods of carbon nanodots synthesis such as the laser ablation of graphite,[11] electrochemical oxidation of graphite or multiwalled carbon nanotubes,[14,15] the microwave pyrolysis of saccharide (e.g., glucose) solution in the presence of poly(ethylene glycol),[13,16,17]

hydrothermal treatment of glucose[18] or orange juice,[19] and heating method of banana juice[20] may involve severe synthetic conditions, a long consumption time, expensive starting materials, low yields, and inconvenient postsynthetic treatments. In addition, such synthesis methods include post-treatment steps with surface passivating agents to functionalize the carbon nanodots and further innovations to dramatically improve their current luminescence efficiencies and photo-stability while decreasing their cytotoxicity.[6] Several chemical approaches are being increasingly used to prevent the use of high-energy systems, post-treatment processing, and expensive precursors.[11−22] Therefore, a simple and convenient method which uses natural precursors to synthesize "green carbon nanodots (G-dots)," which would enable us to use carbon nanodots with high efficiency in an environmentally friendly. The synthesis method of carbon nanodots on a large scale in a cost-effective manner is very useful for biomedical or energy industrial applications.[21] However, there are a very limited number of reports on the green approach of producing fluorescent C-dots from saccharides,[16,17] glucose,[18] and coffee grounds[7] that have been published suffer from drawbacks such as broad size distribution, expensive processing, small scale synthesis, and low chemical stability.

Here, we first report a new large-scale synthesis method of the G-dots from waste food using ultrasound irradiation at room-temperature, which show excellent photoluminescence properties, high photostability, size uniformity, and low cytotoxicity required for biomedical applications. The G-dots were synthesized from large amounts of food waste as renewable sources through our simple processing, including dehydration, polymerization, carbonization, and passivation.[3,6,22] Initially, The food waste is composed with combinations of many organic molecules based on hydrogen bonding. The dehydration, polymerization, and carbonization sequentially occur while the ultrasound irradiation, thereby resulting in a short single burst of nucleation. The resulting nuclei then grow by the diffusion of solutes toward the carbon nanoparticle surfaces. The surfaces of these carbon nano-particles are highly functionalized (G-dots) and do not need any further submodification. Significantly, we describe the design of a new "green solution" for the disposal of waste (Figure 1). Ultimately, high-quality carbon materials G-dots are synthesized from food waste sources, unveiling the usefulness of waste.

■ EXPERIMENTAL SECTION

2.1. Regents. All the regents were purchased from Sigma-Aldrich (Milwaukee, WI, USA). Dulbecco's Modified Eagle's medium (DMEM), RPMI-1640, fetal bovine serum (FBS), antibiotic-antimycotic, L-glutamine, and nonessential amino acids were obtained from Biowest (Lewes, U.K.). Ultrapure water (18.2 MΩ cm^{-1}) from a Milli-Q ultrapure system was used in this study. The pH values of phosphate buffer solutions are 3.0−10.0. Phosphate buffered saline (PBS; 1×, 1 L, pH 7.4) contained NaCl (8 g), KCl (0.2 g), Na$_2$HPO$_4$ (1.44 g), and KH$_2$PO$_4$ (0.24 g).

2.2. Environmentally Friendly Synthesis of G-Dots. The food wastes/ethanol (100 kg of food wastes per 500 L of 10% ethanol) solution was treated for 45 min with ultrasound at 40 kHz (Ultrasonics UC-05, Lab Companion, Korea). The solution was then centrifuged at 4500 rpm for 5 min to remove large or agglomerated particles. The supernatant containing G-dots was filtered twice through a 0.22 μm membrane to further remove large particles, and finally dried at 45 °C.

2.3. Characterization. The morphology and size of G-dots were analyzed by atomic force microscopy (AFM, VEECO Instrument, USA) and high-resolution transmission electron microscopy
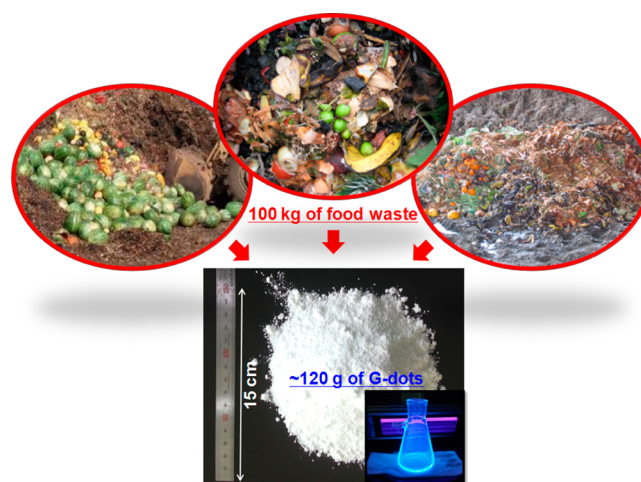

Figure 1. Schematic description of the large-scale synthesis of G-dots. These nanodots represent the efficient transition from large food waste to valuable carbon-based nanomaterials.

(HRTEM, JEM 2200, Japan). For the AFM analysis, 100 μL of the G-dots solution was placed on a silicon wafer. The silicon wafer was air-dried overnight, and the remaining solution was dispersed using an air-gun. The HRTEM specimens were prepared by drop-casting 10 μL of the G-dots solution on a 300 mesh carbon-coated copper TEM grid with a carbon film followed by drying at room temperature. The G-dot crystalline structure was investigated by X-ray diffraction (XRD; Rigaku RDA-cA X-ray diffractometer, Japan) using Cu Kα radiation and a nickel filter. A Raman microscopy system (NT-MDT NTEGRA system, USA) was used to analyze the air-dried G-dots coated on a silica wafer. Fourier transform infrared (FT-IR) spectra were collected on a JASCO FT-IR 470. Each spectrum was recorded from 4000 to 650 cm^{-1} using 12 scans at a resolution of 4 cm^{-1}. The absorption spectrum of G-dots was measured by UV−vis spectrophotometry (UV-1800, Shimadzu, Japan). Photoluminescence (PL) spectroscopy with a changeable UV transilluminator (DUT-260, Core Bio System, Korea) was used to measure the amount of G-dots. The internal quantum yield (QY, 3 mg/mL) of G-dots was measured spectrofluorometer (FP-8500, Jasco, Japan). X-ray photoelectron spectroscopy (XPS), with monochromatic Al Kα X-ray radiation operated at 120 W (Kratos Analytical, AXIS Nova, Manchester, U.K.), was investigated the surface functional properties of the samples. The shift of the binding energy was corrected at 284.6 eV of C1s level.

2.4. Cytotoxicity Testing of the G-Dots. The cytotoxicity of the G-dots was evaluated by the MTT assay. Briefly, Chinese hamster ovary cells (CHO-K1), mouse muscle cells (C2C12), and African green monkey kidney cells (COS-7) cells were seeded in a 96-well plate at a density of 1 × 10^4 cells per well, and cultured in a humidified incubator at 37 °C for 24 h under a 5% CO$_2$ atmosphere in DMEM and/or RPMI-1640 supplemented with 10% FBS and 1% antibiotics. Fresh medium containing an increasing concentration of G-dots was added to each well and incubated for 24 and 72 h. Then, 20 μL of a 0.2 mg mL^{-1} MTS solution in DMEM and/or RPMI-1640 was added to each well and incubated at 37 °C for 2 h. Finally, the optical density was measured at 490 nm with an absorbance microplate reader (EMax microplate reader, Bucher Biotec AG, Basel, Switzerland).

2.5. Cell Imaging. HepG2 cells were cultured in high-glucose DMEM supplemented with 10% FBS, 100 μg mL^{-1} penicillin, and 100 μg mL^{-1} streptomycin. In the proliferative period, HepG2 cells (~1 × 10^5 cell mL^{-1}) were dispersed in 12 replicate wells to a total volume of 100 μL per well and maintained at 37 °C under a 5% CO$_2$/95% air atmosphere in incubator for 24 h. Then, the culture media was removed, and the cells were incubated in culture medium containing the G-dots at different concentrations for 24 h and washed with the culture medium. The fluorescence images were obtained using a confocal microscope (LSM 510META; Carl Zeiss) with Ar ion, and HeNe lasers.
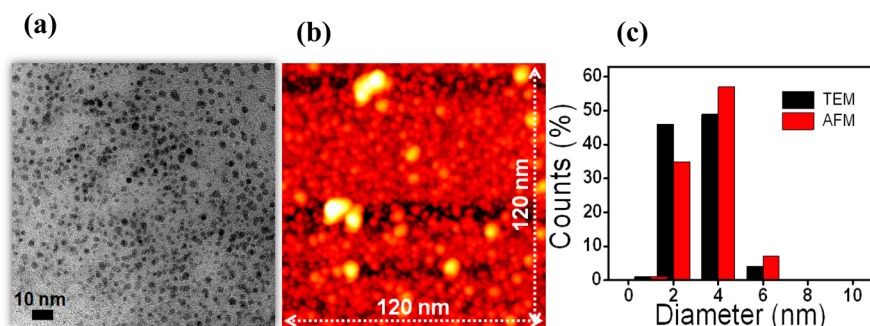
Figure 2. (a) HR-TEM image, (b) AFM image, and (c) the size distribution of G-dots.
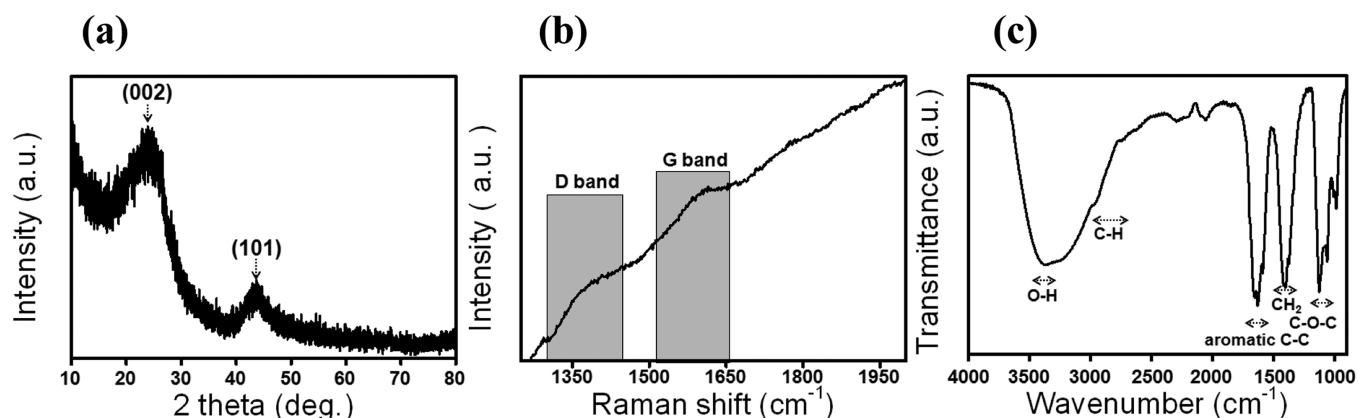

Figure 3. Physicochemical characteristics of G-dots: (a) XRD pattern, (b) Raman spectrum, (c) FTIR spectrum.

2.6. Plant Germination and Growth on the Byproducts (Not Including G-Dots) of G-Dot Synthesis from Large Food-Waste-Derived Sources. Seeds of *Laphanus sativus L.* were sterilized by a 10 min treatment with 50% Chlorox solution and then rinsed 5 times with sterile water. Sterile *Laphanus sativus L.* seeds were placed on a gauze moistened with 3DW supplemented with different concentrations of residues (0, 2, and 10 mg mL^{-1}) for germination and growth. Sterile magenta boxes were used for all the germination and growth experiments.

■ RESULTS AND DISCUSSION

3.1. Physicochemical, Structural, and Optical Properties of G-Dots. The G-dots synthesized from food waste-derived sources were characterized as follows. The morphology of the G-dots (Figure 2) was assessed using TEM and AFM. A few drops of a dilute aqueous solution of G-dots were deposited on a carbon-coated copper grid for TEM and on glass and silicon substrates for AFM. The images revealed that the nanoparticles had a uniform spherical shape with a diameter of 1−7 nm, with most of the particles being 4 nm wide. The average particle size of G-dot determined from the TEM and AFM images was about 4.6 nm.

Figure 3a, which displays the XRD pattern of G-dots, shows an intense peak at $2\theta = 24.7°$ and a weak peak at $2\theta = 43.3°$ that are assigned to (002) and (101) diffraction patterns of graphitic carbon, respectively.[20−22] The former peak corresponds to the interlayer spacing of ∼3.77 Å, which is slightly longer than the spacing between the (002) planes in bulk graphite (3.44 Å). The Raman spectra of the G-dots display 2 broad peaks at around 1365 and 1575 cm^{-1}, which are attributed to the D band (sp^3-hybridized) and G band (sp^2-hybridized) of graphite, respectively (Figure 3b).[23,24] The D band is associated with the vibrations of carbon atoms with

dangling bonds in the termination plane of disordered graphite.[24] The G band corresponds to the E_{2g} mode of graphite and is related to the vibration of the sp^2-hybridized carbon atoms in a two-dimensional hexagonal lattice.[23,24] For the C dots, the relative intensity of the disordered D band and crystalline G band (I_D/I_G) is around 0.88, thus indicating that they have a structure similar to graphite. FTIR analysis of G-dots revealed the following (Figure 3c): the vibrations of the −OH, C−O−C, C−C, and C−H bonds, asymmetric and symmetric stretching vibrations of C−O−C (around 1,300 and 1,200 cm^{-1}) and C−O stretching vibrations were detected, indicating a partial oxidation of the G-dot surface.[3,17,22−24] The broad absorption bands at 3400 cm^{-1} were assigned to O−H. The presence of functional groups containing −OH, which can be used as the linker for the attachment of biomolecules (e.g., DNA, RNA, protein, and cell).[22−24] Figure S1 in the Supporting Information shows the X-ray photoelectron spectroscopy (XPS) data for chemical composition, atomic ratio, and relative areas of the functional groups by deconvoluting the C1s peaks. Based on C1s peak binding energies of 284.7, the G-dots showed the −C−O (286.2 eV), C−O−C═O (287.3 eV), and O═C−O−H (288.9 eV) peaks in the C1s spectrum. These functional groups improve the solubility and stability of the G-tags in an aqueous system.

These functional groups improve the hydrophilicity and stability of the G-dots in an aqueous system. The G-dots exhibit very good solubility in water because of the abundant oxygen-containing groups or hydrophilic groups (e.g., −OH, C−O−C) around the surface. The presence of oxygen-containing functional groups offers options for various types of surface modifications, which will increase the surface properties the
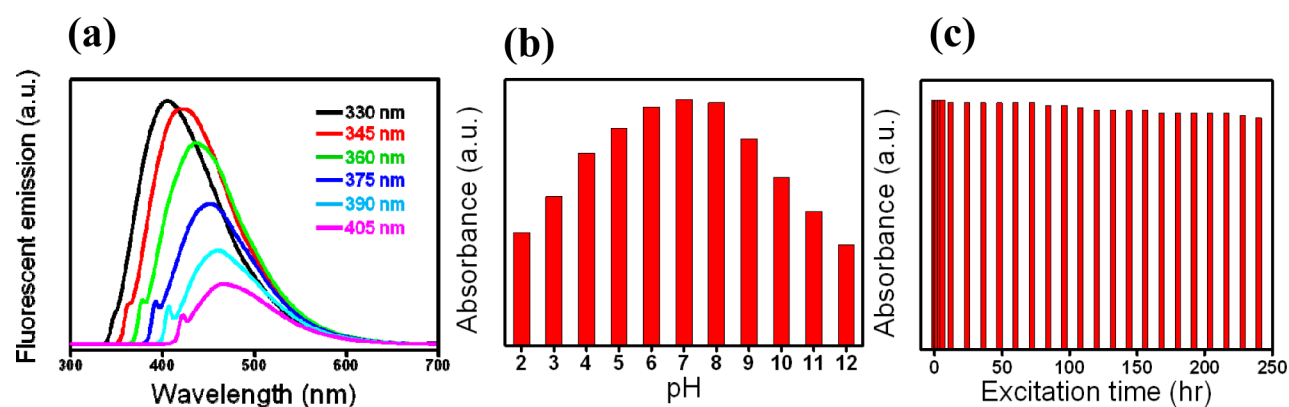
3367

dx.doi.org/10.1021/am500159p | *ACS Appl. Mater. Interfaces* 2014, 6, 3365−3370

Figure 4. Photoluminescence (PL) results of G-dots. (a) PL emission spectra of G-dots obtained at a 198 mJ/pulse for 30 min with different excitation wavelengths increasing from 330 to 405 nm in 20 nm increments. (b) Effect of the solution pH on the G-dot fluorescence intensity. (c) Dependence of the fluorescence intensity on the excitation time in 3DW.

potential to be used for application in various areas, including drug delivery, biosensing, and biomedical imaging.

Figure S2 in the Supporting Information shows aborption spectrum of G-dots (1 mg/mL) in aqueous solution, exhibiting absorption intensity at <400 nm. Figure 4a displays the emission spectra of G-dots, which have a small range from blue (400 nm) to red (470 nm), depending on the excitation wavelength. The different excitation wavelengths might affect the subsequent excited state energy distribution, the charge separation, and/or the confinement of electrons and holes on the G-dot surface and their radiative recombination.[15−22] Therefore, the narrow photoluminescence emission area (400−470 nm) confirms that the size distribution of the G-dots (2−5 nm) is small because of similar quantum effects and emission traps on the surfaces, showing 2.85% internal quantum yield (QY), as supported by the TEM and AFM images (Figure 2). As the excitation wavelength increases, the emission peak position shifts to longer wavelengths and the intensity decreases. We found that the intensity decreased when the pH value of the solution was higher or lower than 7. However, this change was nullified when the pH value was adjusted back to this optimal value (Figure 4b). We also observed that the photoluminescence intensity of the G-dots derived from large food waste-derived sources was maximal at pH 7, and the intensity was decreased significantly (a 40−62% decrease) with a slight blue shift upon changing to either an acidic or a basic solution. To investigate the photostability of the G-dots, we analyzed their photoluminescence for 10 days (Figure 4c). The G-dots had excellent photostability; their photoluminescence intensity decreased slowly (∼8%) under continuous excitation with a Xe lamp for 10 days. These results reveal that the G-dots have great potential in protein (or DNA and RNA)-labeling and bioimaging studies.

3.2. Cytotoxicity by Introducing G-Dots in Cells. Low cytotoxicity is one of the most critical requirements for an ideal multifunctional biomaterial with the capacity to be used in bioimaging.[6,22] To evaluate the cytotoxicity of the G-dots, the relative viabilities of CHO-K1, C2C12, and COS-7 cells exposed to G-dots were measured using the MTT assay (Figure 5). Figure 5 shows the cell viability after incubation with G-dots at a concentration of 0−4 mg mL^{-1} for 24 h. After 24 h of incubation, the cell viability decreased to less than 17% when concentrations of 4 mg mL^{-1} of G-dots were used. These observations clearly indicated that, over a period of 24 h, G-dots (at a concentration up to 2 mg mL^{-1} did not exert any
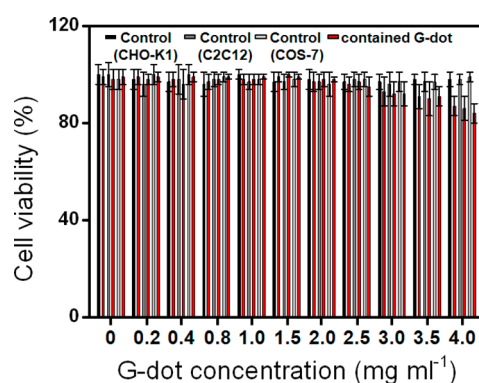

Figure 5. Cytotoxicity of G-dots at increasing concentrations, from 0 to 4 mg mL^{-1}, on Chinese hamster ovary cell (CHO-K1), mouse muscle cell (C2C12), and African green monkey kidney cell (COS-7) cells.

cytotoxic effects on the cell lines. Beyond this concentration, the cell viability gradually decreased in a concentration-dependent manner. Importantly, at the concentrations typically used in bioimaging applications (<2 mg mL^{-1}), the cytotoxicity of the G-dots was found to be marginal. For further incubation at 72 h, G-dots showed still negligible cytoxotic effects (see Figure S3 in the Supporting Information).

3.3. In Vitro Bioimaging of G-Dots. Because of their photostability, high water solubility, and low toxicity, G-dots are an attractive alternative for bioimaging.[22] To determine if G-dots could be used in living systems, we performed fluorescence imaging of human hepatocellular liver carcinoma (HepG2) cells treated with 0−2 mg mL^{-1} G-dots. The cultured HepG2 cells were incubated with G-dots in the culture medium for 30 min at 37 °C. Then, the G-dots were monitored by confocal microscope. Figures 6a,c and b,d show the confocal microscopic images of HepG2 cells after incubation with 0.5 and 1 mg mL^{-1} G-dots, respectively. The HepG2 cells treated with G-dots showed no substantial change in shape. A strong red-colored photoluminescence in the nuclei indicated that the G-dots penetrated into the cells and maintained their fluorescent properties in the cellular environment, while the photoluminescence in the cytoplasm was very weak. The control cells with no treated of the G-dots showed no red photoluminescence at the same exposure conditions.

3.4. Plant-Growth-Promoting Effects of the Byproducts (Not Including G-Dots) of G-Dot Synthesis from
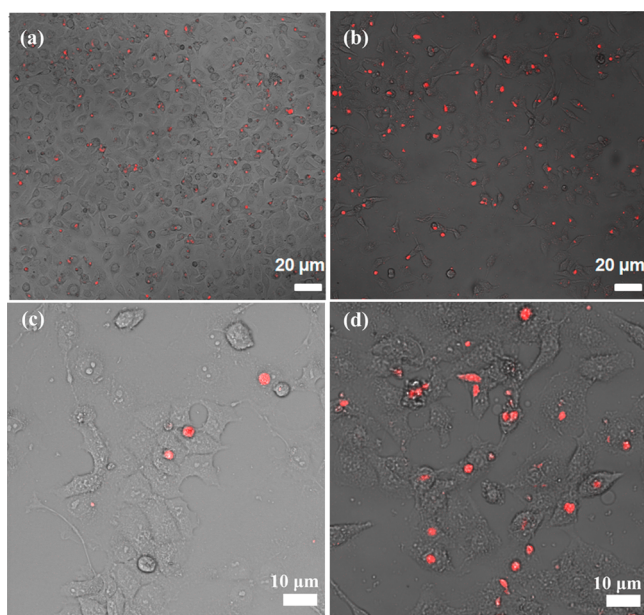
Figure 6. Confocal microscopy images of HepG2 cells treated with G-dots at concentrations of (a, c) 0.5 and (b, d) 1 mg mL^{-1}.

Large Food-Waste-Derived Sources. We consequently observed that G-dots could enter the cells without any further fuctionalization. Thus, this in vitro investigation demonstrates an immense potential of G-dots for bioimaging applications. We further investigated the effects of the byproducts (not including G-dots) of G-dot synthesis from large food-waste derived sources on the growth and development of seedlings germinated on 3DW-supplemented gauze. We placed sterile *Laphanus sativus L.* on gauze (moistened with 3DW) supplemented with different concentrations of the byproducts (0, 2, and 10 mg mL^{-1}). As shown in Figure 7a, the addition of the byproducts to gauze was found to accelerate the process of seed germination and significantly shortened the germination time. *Laphanus sativus L.* placed on gauze with 2 and 10 mg mL^{-1} byproducts nearly germinated within 30 h, whereas no

germination in the same time period was observed for *Laphanus sativus L.* seeded on the gauze treated with 0 mg mL^{-1} of the byproducts. The germination rates during the 30 h observation period were dramatically higher for *Laphanus sativus L.* treated with the byproducts than that in the absence of the byproducts. The germination percentage for the seeds that were placed on a regular gauze (moistened with 3DW) averaged 4% in 18 h and 9% in 30 h, whereas the germination percentage of the seeds placed on gauze supplemented with 1 mg mL^{-1} the byproducts averaged 43% in 18 h and 91% in 30 h (Figure 7a). Seedlings with developed cotyledons and a root system were recognized as fully germinated in this experiment. We further investigated the effects of the byproducts on the growth and development of the seedlings germinated on gauze supplemented with the byproducts. *Laphanus sativus L.* seedlings germinated and developed on the medium with different concentrations of the byproducts (2 and 10 mg mL^{-1}) exhibiting a dramatic increase in the vegetative biomass (data not shown). The fresh length (from root to stem) of *Laphanus sativus L.* seedlings germinated and grown on the byproducts containing gauze increased by 11.1-fold compared with those placed on the 3DW-moistened regular gauze (Figure 7b). Compared to the control seedlings, the byproducts-exposed *Laphanus sativus L.* seedlings had longer stems and were more developed. These findings highlight the plant growth-promoting effects of the byproducts (not including G-dots) of G-dot synthesis from large food-waste derived sources.

CONCLUSION

In summary, we first developed a green chemical approach for the synthesis of photoluminescent G-dots from food waste using ultrasound irradiation at room-temperature. To the best of our knowledge, this is the first example of the large-scale synthesis of G-dots from food waste-derived sources. About 120 g of G-dots (size 2−4 nm) per 100 kg of food waste can be produced by our simple and green approach. The G-dots exhibit very good solubility in water because of the presence of abundant oxygen-containing groups on their surfaces. The G-dots have excellent photostability and low cytotoxicity (<2 mg
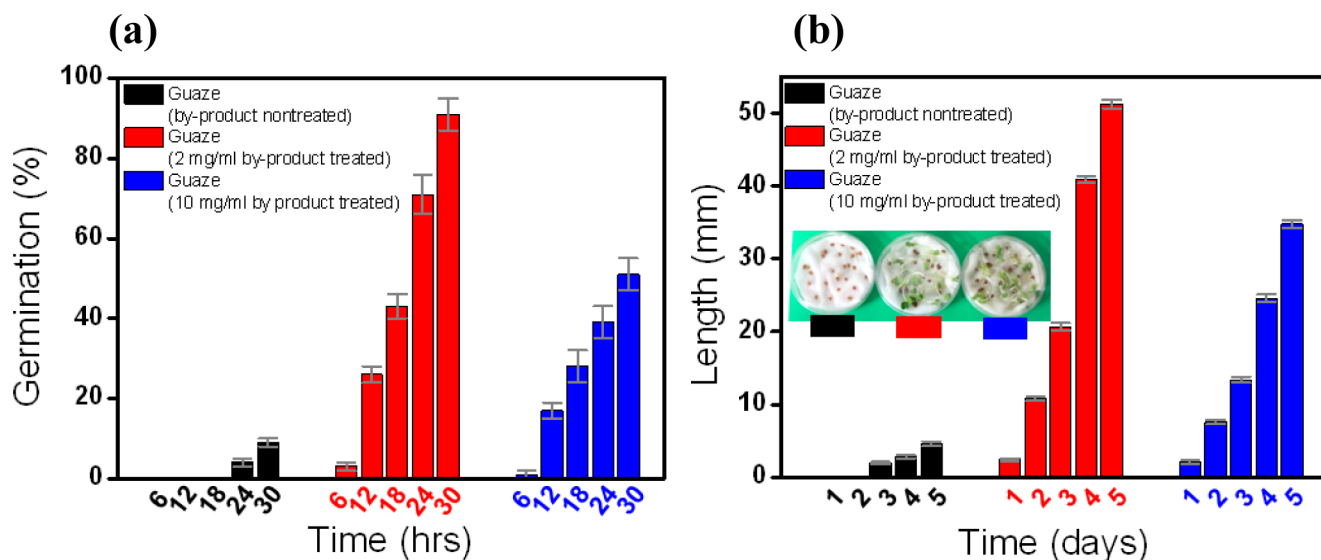

Figure 7. Effect of the byproducts (not including G-dots) of G-dot synthesis from large food-waste-derived sources on (a) the germination and (b) growth of *Laphanus sativus L.* seedlings.

mL^{-1}). The in vitro bioimaging results demonstrate an immense potential for biomedical application. In addition, the byproducts (not including G-dots) of food waste could promote the growth and development of seedlings germinated on 3DW-supplemented gauze. Thus, G-dots and byproducts (not including G-dots) of G-dot synthesis from large food-waste derived sources show great promise for application in biomedical imaging and plant seed germination and/or growth, respectively.

■ ASSOCIATED CONTENT

Ⓢ Supporting Information

XPS data of G-dots showed in Figure S1. UV−vis absorption spectrum of G-dots presented in Figure S2. Cytotoxicity of G-dots at 72 h exhibited in Figure S3. This material is available free of charge via the Internet at http://pubs.acs.org/.

■ AUTHOR INFORMATION

Corresponding Authors

*E-mail: leeho@kbsi.re.kr. Tel.: +82-42-865-3637; Fax: +82-42-865-3610.
*E-mail: jouhahn@kbsi.re.kr. Tel.: +82-42-865-3613. Fax: +82-42-865-3610.

Author Contributions

[†]These authors contributed equally to this work.

Notes

The authors declare no competing financial interest.

■ ACKNOWLEDGMENTS

■ REFERENCES

(1) Zhou, L.; Lin, Y.; Huang, Z.; Ren, J.; Qu, X. Carbon Nanodots as Fluorescence Probes for Rapid, Sensitive, and Label-free Detection of Hg^{2+} and Biothiols in Complex Matrices. *Chem. Commun.* **2012**, *48*, 1147−1149.

(2) Yuan, L.; Lin, W.; Yang, Y.; Chen, H. A Unique Class of Near-Infrared Functional Fluorescent Dyes with Carboxylic-Acid-Modulated Fluorescence ON/OFF Switching: Rational Design, Synthesis, Optical Properties, Theoretical Calculations, and Applications for Fluorescence Imaging in Living Animals. *J. Am. Chem. Soc.* **2012**, *134*, 1200−1211.

(3) Jeong, J.; Jung, J.; Choi, M.; Kim, J. W.; Chung, S. J.; Lim, S.; Lee, H.; Chung, B. H. Color-Tunable Photoluminescent Fullerene Nanoparticles. *Adv. Mater.* **2012**, *24*, 1999−2003.

(4) Qian, J.; Wang, D.; Cai, F. H.; Xi, W.; Peng, L.; Zhu, Z. F.; He, H.; Hu, M. L.; He, S. Observation of Multiphoton-Induced Fluorescence from Graphene Oxide Nanoparticles and Applications in In Vivo Functional Bioimaging. *Angew. Chem., Int. Ed.* **2012**, *51*, 10570−10575.

(5) Duque, J. G.; Hamilton, C. E.; Gupta, G.; Crooker, S. A.; Crochet, J. J.; Mohite, A.; Htoon, H.; Obrey, K. A. D.; Dattelbaum, A. M.; Doorn, S. K. Fluorescent Single-Walled Carbon Nanotube Aerogels in Surfactant-free Environments. *ACS Nano* **2011**, *5*, 6686−6694.

(6) Baker, S. N.; Baker, G. A. Luminescent Carbon Nanodots: Emergent Nanolights. *Angew. Chem., Int. Ed.* **2010**, *49*, 6726−6744.

(7) Akhter, S.; Ahmad, I.; Ahamd, M. Z.; Ramazani, F.; Singh, A.; Rahman, Z.; Ahmad, F. J.; Storm, G.; Kok, R. J. Nanomedicines as Cancer Therapeutics: Current Status. *Curr. Cancer Drug Targets* **2013**, *13*, 362−378.

(8) Hsu, P. C.; Shih, Z. Y.; Lee, C. H.; Chang, H. T. Synthesis and Analytical Applications of Photoluminescent Carbon Nanodots. *Green Chem.* **2012**, *14*, 917−920.

(9) Yang, S. T.; Cao, L.; Luo, P. G.; Lu, F.; Wang, X.; Wang, H.; Meziani, M. J.; Liu, Y.; Qi, G.; Sun, Y. P. Carbon Dots for Optical Imaging in Vivo. *J. Am. Chem. Soc.* **2009**, *131*, 11308−11309.

(10) Peng, H.; Travas-Sejdic, J. Simple Aqueous Solution Route to Luminescent Carbogenic Dots from Carbohydrates. *Chem. Mater.* **2009**, *21*, 5563−5565.

(11) Sun, Y. P.; Zhou, B.; Lin, Y.; Wang, W.; Fernando, K. A. S.; Pathak, P.; Meziani, M. J.; Harruff, B. A.; Wang, X.; Wang, H.; Luo, P. G.; Yang, H.; Kose, M. E.; Chen, B.; Veca, L. M.; Xie, S. Y. Quantum-Sized Carbon Dots for Bright and Colorful Photoluminescence. *J. Am. Chem. Soc.* **2006**, *128*, 7756−7757.

(12) Li, Q.; Ohulchanskyy, T. Y.; Liu, R.; Koynov, K.; Wu, D.; Best, A.; Kumar, R.; Bonoiu, A.; Prasad, P. N. Photoluminescent Carbon Dots as Biocompatible Nanoprobes for Targeting Cancer Cells in Vitro. *J. Phys. Chem. C* **2010**, *114*, 12062−12068.

(13) Liu, C.; Zhang, P.; Tian, F.; Li, W.; Li, F.; Liu, W. One-step Synthesis of Surface Passivated Carbon Nanodots by Microwave Assisted Pyrolysis for Enhanced Multicolor Photoluminescence and Bioimaging. *J. Mater. Chem.* **2011**, *21*, 13163−13167.

(14) Zhao, Q. L.; Zhang, Z. L.; Huang, B. H.; Peng, J.; Zhang, M.; Pang, D. W. Facile Preparation of Low Cytotoxicity Fluorescent Carbon Nanocrystals by Electrooxidation of Graphite. *Chem. Commun.* **2008**, *41*, 5116−5118.

(15) Lu, J.; Yang, J. X.; Wang, J.; Lim, A.; Wang, S.; Loh, K. P. One-pot Synthesis of Fluorescent Carbon Nanoribbons, Nanoparticles, and Graphene by the Exfoliation of Graphite in Ionic Liquids. *ACS Nano* **2009**, *3*, 2367−2375.

(16) Lee, C. H.; Rajendran, R.; Jeong, M. S.; Ko, H. Y.; Joo, J. Y.; Cho, S.; Chang, Y. W.; Kim, S. Bioimaging of Targeting Cancers using Aptamer-conjugated Carbon Nanodots. *Chem. Commun.* **2013**, *49*, 6543−6545.

(17) Sun, X.; Li, Y. Colloidal Carbon Spheres and Their Core/Shell Structures with Noble-metal Nanoparticles. *Angew. Chem., Int. Ed.* **2004**, *43*, 597−601.

(18) Yang, Z. C.; Wang, M.; Yong, A. M.; Wong, S. Y.; Zhang, X. H.; Tan, H.; Chang, A. Y.; Li, X.; Wang, J. Intrinsically Fluorescent Carbon Dots with Tunable Emission Derived from Hydrothermal Treatment of Glucose in the Presence of Monopotassium Phosphate. *Chem. Commun.* **2011**, *47*, 11615−11617.

(19) Sahu, S.; Behera, B.; Maiti, T.; Mohapatra, S. Simple One-step Synthesis of Highly Luminescent Carbon Dots from Orange Juice: Application as Excellent Bio-imaging Agents. *Chem. Commun.* **2012**, *48*, 8835−8837.

(20) De, B.; Karak, N. A Green and Facile Approach for the Synthesis of Water Soluble Fluorescent Carbon Dots from Banana Juice. *RSC Adv.* **2013**, *3*, 8286−8290.

(21) kumar, V.; Toffoli, G.; Rizzolio, F. Fluorescent Carbon Nanoparticles in Medicine for Cancer Therapy. *ACS Med. Chem. Lett.* **2013**, *4*, 1012−1013.

(22) Li, H.; Kang, Z.; Liu, Y.; Lee, S. T. Carbon Nanodots: Synthesis, Properties and Applications. *J. Mater. Chem.* **2012**, *22*, 24230−24253.

(23) Qu, S.; Wang, X.; Lu, Q.; Liu, X.; Wang, L. A Biocompatible Fluorescent Ink Based on Water-Soluble Luminescent Carbon Nanodots. *Angew. Chem., Int. Ed.* **2012**, *124*, 12381−12384.

(24) Mewada, A.; Pandey, S.; Shinde, S.; Mishra, N.; Oza, G.; Thakur, M.; Sharon, M.; Sharon, M. Green Synthesis of Biocompatible Carbon Dots using Aqueous Extract of Trapa Bispinosa Peel. *Mater. Sci. Eng., C* **2013**, *33*, 2914−2917.